Heliyon 8 (2022) e09167

Contents lists available at ScienceDirect

Heliyon

journal homepage: www.cell.com/heliyon

Research article

Natural killer cells activity against multiple myeloma cells is modulated by osteoblast-induced IL-6 and IL-10 production

Christopher Uhl [a], Themba Nyirenda [b], David S. Siegel [a,b], Woo Y. Lee [c,1], Jenny Zilberberg [a,*,1]

[a] Center for Discovery and Innovation, 111 Ideation Way, Building 102, Nutley, NJ 07110, USA
[b] John Theurer Cancer Center, 92 2nd St Ste 301 Hackensack, NJ 07601, USA
[c] Department of Chemistry and Chemical Biology, Stevens Institute of Technology, 1 Castle Point on Hudson, Hoboken, NJ, 07030, USA

ARTICLE INFO

Keywords:
NK cells
Multiple myeloma
Cytotoxicity
Osteoblasts
Microenvironment

ABSTRACT

Background: Natural killer (NK) cells are part of the innate arm of the immune system; as such NK cells can be activated rapidly to target virus-infected cells and tumor cells without prior sensitization. The human NK-92MI cell line is among the most widely used NK cell in preclinical research studies and has also been approved for clinical applications. Previous studies have shown that osteoblasts (OSB) confer drug resistance in multiple myeloma (MM) and other cancers that metastasize to the bone marrow.

Aim: We evaluated here how OSB, which are bone forming cells and a key cellular component of the bone marrow microenvironment, modulate the cytotoxic activity of NK-92MI cells against the MM.1S multiple myeloma cell line.

Methods: The osteoblastic niche was recapitulated with either the osteoblastic cell line hFOB 1.19 (hFOB) or primary osteoblasts (P-OSB) derived from surgical resections. Time-lapse imaging was utilized to quantify changes in MM.1S cell viability under different conditions, including: (1) Co-culture of MM.1S with NK92MI cells, (2) triple-culture of hFOB or P-OSB with MM.1S and NK-92MI, and (3) MM.1S or NK-92MI cells primed with OSB-derived supernatant. Cytokine analysis was conducted to quantify potential secreted factors associated with the protective effects of OSB.

Results: The physical presence of OSB hindered the activity of NK-92MI cells, resulting in the increased viability of MM.1S compared to co-cultures which lacked OSB. This observation was accompanied by reduced perforin and granzyme A secretion from NK-92MI cells. Contact of OSB and NK-92MI cells also induced interleukin 6 (IL-6) and interleukin 10 (IL-10) production; two cytokines which are known to impair the NK cell immunity against MM and other cancers. OSB supernatant also conferred cytoprotection to MM.1S, suggesting a dual mechanism by which OSB may modulate both NK and MM cells.

Conclusions: We demonstrated here that OSB can negatively impact the activity of NK cells against MM. As NK cells and their chimeric antigen receptor-modified versions become more widely used in the clinic, our results suggest that understanding the role of OSB as potential immunoregulators of the NK cell-mediated cytotoxic response in the bone marrow tumor microenvironment may provide new opportunities for enhancing the effectiveness of this potent immunotherapeutic approach.

1. Introduction

Multiple myeloma (MM) is a B-cell malignancy characterized by the accumulation of monoclonal malignant plasma cells in the bone marrow, the presence of high levels of monoclonal serum antibody, and the development of anemia, renal insufficiency, and osteolytic bone lesions [1]. Despite the development of novel therapies which target not only MM cells but also their interplay with the microenvironment, MM remains an incurable disease [1]. It is well established that bone fosters the dormancy and progression of MM cells, which in turn interact with the bone niche to colonize, evade therapy, and dysregulate bone homeostasis [2]. In particular, the bone-lining endosteal layer at the bone/bone marrow (BM) interface fosters the survival of drug-resistant MM cells, in part through their interactions with osteoblasts (OSB) [3]. We previously

* Corresponding author.
E-mail address: jenny@discordia.org (J. Zilberberg).
[1] Equal contributors.

https://doi.org/10.1016/j.heliyon.2022.e09167
Received 8 August 2021; Received in revised form 29 November 2021; Accepted 18 March 2022

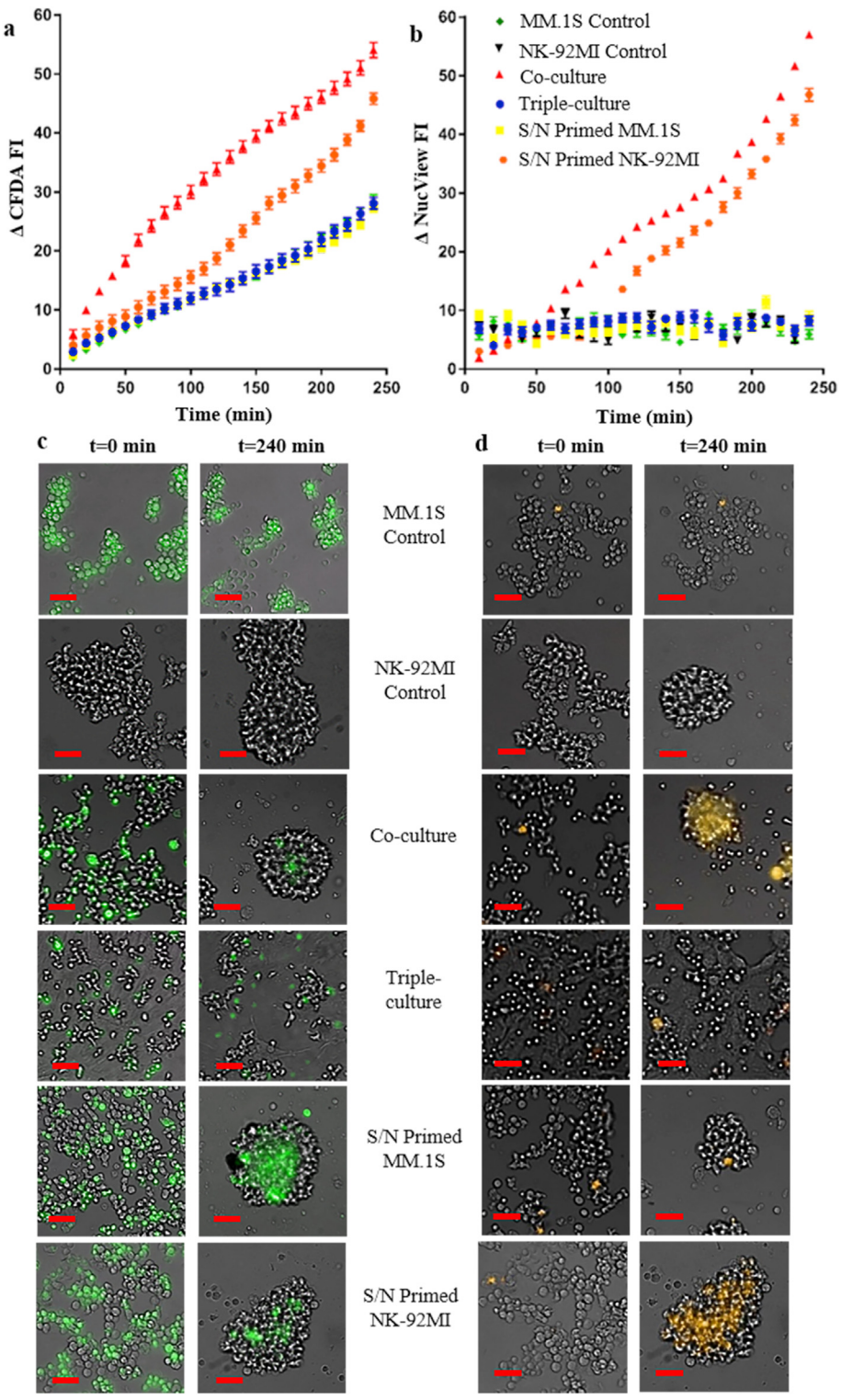

Figure 1. Viability of MM.1S cells quantified via changes in CFDA-SE (live) and NucView (apoptotic) FI signals in cultures with hFOB cells. (a) Change in CFDA-SE FI. (b) Change in NucView FI. (c) Representative brightfield and CFDA-SE (green) image composites. (d) Representative brightfield, CFDA-SE (green), and NucView (red) image composites with scale bars = 150 μm long. 5-10 separate image sets were collected per experimental condition. Two-way ANOVA and Dunnett's multiple comparisons are summarized in Table 1.

reported that MM cells co-cultured with OSB acquired resistance to bortezomib [4], a proteasome inhibitor widely used for the treatment of this disease. Based on these results, we sought to investigate if OSB could also modulate the cytotoxic activity of natural killer (NK) cells against MM cells.

NK cells are a type of lymphocyte that belong to the innate immune system [5]. Their effector functions are regulated by the surface expression of inhibitory and activating receptors. Unlike cytotoxic T cells, NK cells can recognize tumor cells that lack the expression of major histocompatibility complex class I molecules [6]. This cytotoxic mechanism has driven the exploration of NK cells' role in the biology and treatment of MM and other cancers [7, 8, 9, 10]. In this brief communication we report, for the first time, that OSB are capable of shaping the anti-myeloma response of NK cells in part through cytokine regulation. As the next-generation of NK cell-based immunotherapies, such as ex vivo expanded killer cell immunoglobulin-like receptor (KIR)-mismatched NK cells and chimeric antigen receptor (CAR)-NK cells enters the clinical space [7, 11], our results suggest the need to further explore

Table 1. Statistical analyses for Figure 1.

Condition vs MM.1S Control	10–120 min	130–240 min	10–120 min	130–240 min
	ΔCFDA Signal		ΔNucView Signal	
NK-92MI Control	n/a	n/a	ns	ns
Co-culture	s****	s****	ns	s****
Triple-culture	ns	ns	ns	ns
S/N Primed MM.1S	ns	ns	ns	ns
S/N Primed NK-92MI	ns	s****	ns	s****

2-way ANOVA and Dunnett's multiple comparisons test. A $p < 0.05$ was considered statistically significant. s - significant difference (****$p < 0.0001$, **$p < 0.01$), ns - not significant, n/a - not applicable (i.e. no CFDA signal). All comparisons were made to the MM.1S controls where cell viability was maintained throughout the experiments. *No significant difference* compared to MM.1S control implies no loss of cell viability. *Significant difference* suggest a departure from control arising from a decrease in cell viability.

the potential immunosuppressive landscape conferred by the tumor microenvironment in order to enhance these potent and promising therapeutic approaches.

2. Materials and methods

2.1. Cell lines and cell culture

To recapitulate the osteoblastic niche, we utilized the osteoblastic cell line hFOB 1.19 (hFOB; ATCC® CRL-11372, derived from fetal tissue) and primary osteoblasts (P-OSB) derived from a patient with osteoarthritis. The base medium for the hFOB cell line was a 1:1 mixture of Ham's F12 Medium and Dulbecco's Modified Eagle's Medium, with 2.5 mM L-glutamine. The complete growth medium consisted of the base medium plus 0.3 mg/ml G418 and fetal bovine serum (FBS) at a final concentration of 10%. As recommended, hFOB cells were maintained at 34 °C and 5% CO_2. P-OSB cells were isolated from discarded surgical samples obtained from an osteoarthritis patient undergoing joint replacement. Bone fragments were subjected to enzymatic dissociation using serial digestions with collagenase type 1A and EDTA. The supernatant from the fourth enzymatic digestion was collected, plated and allowed to proliferate for 14 days before characterization via alkaline phosphatase (ALP) activity [12]. P-OSB were cultured in α-MEM medium supplemented with 10% penicillin–streptomycin (P/S), 10% FBS, 3μM b-glycerophosphate and 50 mg/mL l-ascorbic acid [12].

The NK-92MI cell line (ATCC® CRL-2408) was used as model NK cells. The clinical use of this cell line, established from a 50-year-old male patient with progressive non-Hodgkin's lymphoma [13], is rapidly expanding due to its therapeutic potential as an off-the-shelf third party immunotherapy [6, 14]. NK-92MI cells were cultured in MyeloCult™ H5100 (StemCell Technologies cat # 05150).

MM.1S cell line (ATCC® CRL-2974), an extensively characterized and commonly utilized MM model was originally derived from a 42-year-old patient. It expresses the glucocorticoid receptor and is dexamethasone sensitive [15, 16]. MM.1S cells were cultured following ATCC specifications in RPMI-1640 medium supplemented with 10% FBS. Cells were maintained at 37 °C and 5% CO_2. All cytotoxic assays were performed at 37 °C and 5% CO_2.

2.2. MM.1S labeling

MM.1S cells were pre-stained with 2 μM CFDA-SE (5-(and-6)-Carboxyfluorescein Diacetate, Succinimidyl Ester; Thermo Fisher #V12883) following the manufacture's recommendations for labeling cells in suspension. To this end, the cell pellets were resuspended gently in pre-warmed (37 °C) PBS containing the CFDA-SE and incubated for 15 min at 37 °C. After staining, cells were re-pelleted and resuspend in fresh pre-warmed medium, incubated another 30 min to ensure complete modification of the probe and then wash again in complete medium. To assess cellular apoptosis via caspase-3 staining, NucView (Biotium #10408) was added directly to the cultures to a final concertation of 2 μM, prior to the starting of the assays.

2.3. NK cytotoxicity assay

NK cell cytotoxicity against tumor cells was assed following published protocols [17, 18] with modifications to incorporate the osteoblasts in the cultures. In brief, hFOB or P-OSB cells were seeded in 96 well plates (8×10^3 cells/well) and cultured for 3–4 days until confluent. A 1:1 effector (NK-92MI): target (MM.1S) ratio (5×10^4 cells) was used for all experiments. The following conditions were tested: (1) Triple-culture of hFOB or P-OSB with MM.1S and NK-92MI, (2) co-culture of MM.1S and NK-92MI, (3) co-culture of NK-92MI and OSB supernatant-primed MM.1S cells, (4) co-culture of MM.1S cells and OSB supernatant-primed NK-92MI, (7) MM.1S control (5×10^4 cells), (8) NK-92MI control (5×10^4 cells) and (9) hFOB or P-OSB control. For triple-culture setups, MM cells were incubated for 1 h with OSB prior to adding the NK cells. Likewise, priming of MM or NK cells with supernatant from either hFOB or P-OSB was conducted for 1 h prior to co-cultures. Cytotoxic assays were run for a total of 4 h.

2.4. Time-lapse imaging

Time-lapse imaging was performed using a Nikon Eclipse Ti2 epi-fluorescence scope equipped with a Hamamatsu C13440 digital camera, Nikon 20x Plan Fluor objective, and a TOKAI HIT stage top incubator. Brightfield, FITC, and TRITC image sets were taken every 10 min over 4 h. ImageJ (NIH, bundled with 64-bit Java 1.8.0_112) was used to process the time lapse images for quantification of CFDA-SE and NucView signals. All images captured were sequentially organized to produce time lapse image sets for each location imaged on the well plate. Image sets were broken down in separate sequences of the brightfield, FITC and TRITC images captured at each location. In order to quantify the fluorescence intensity (FI) of the CFDA-SE and NucView signals, regions of interest (ROI) containing the desired signal in each image for all time points, were determined. This was accomplished by first opening one set of CFDA-SE images and using the "Threshold" function to identify the region of each image in the set that was positive for CFDA-SE signal. After overlaying the ROI boundary for each image, ImageJ performs a calculation to quantify the signal intensity of the raw CFDA-SE signal within the bounds of each ROI for all images in a given set. The measurements taken from each image were further analyzed. Identification of the NucView signal being expressed by MM.1S cells also stained with CFDA-SE (i.e., not viable cells) was accomplished by overlaying the CFDA-SE and NucView signals for each individual image in a set and identifying the regions of the image where both signals were colocalized using the "Colocalization" function in ImageJ. The regions with both the green CFDA-SE signal and red NucView signal were selected and saved as ROIs. The ROIs saved for the colocalized signal were then applied to the original image set containing only the NucView signal in

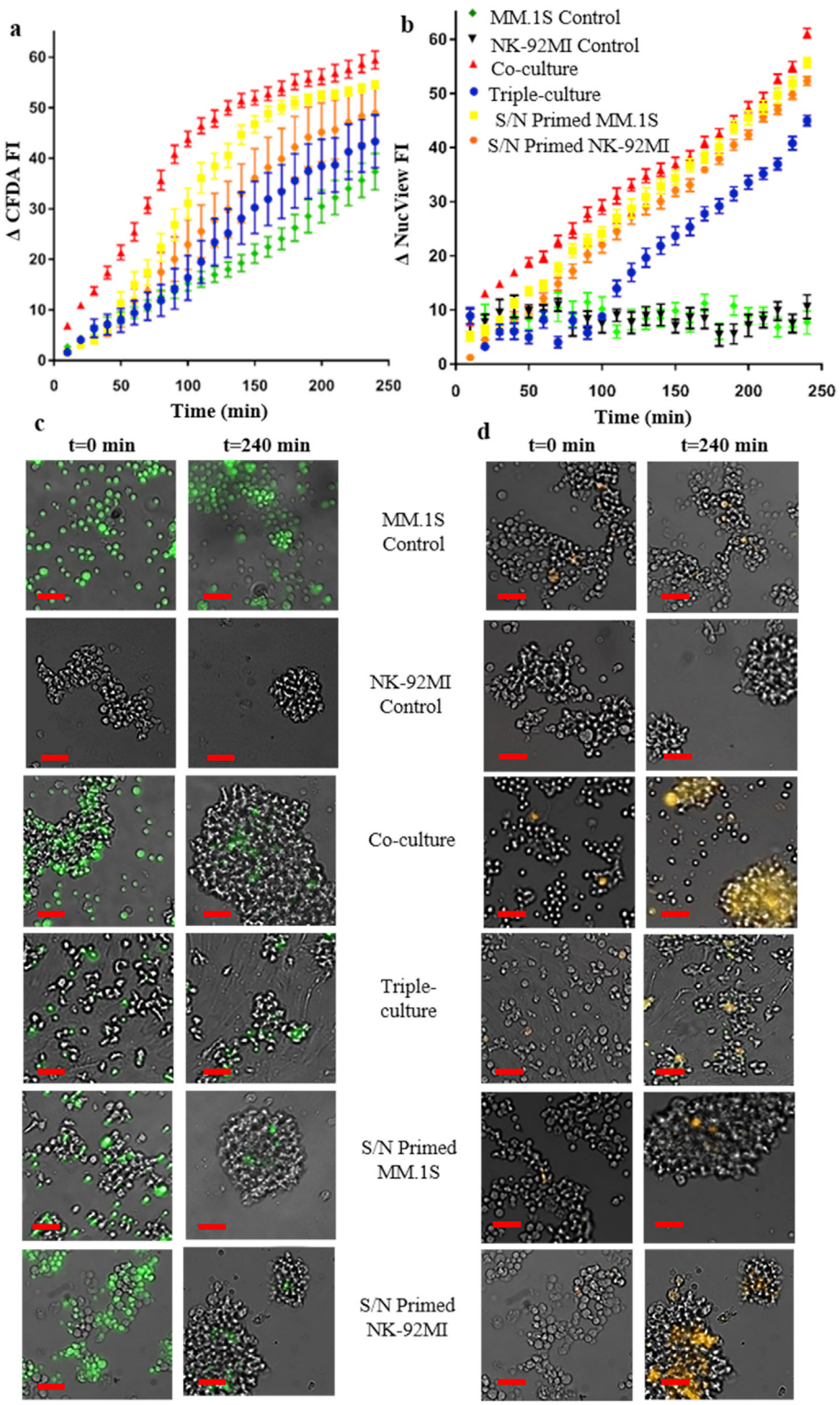

Figure 2. Viability of MM.1S cells quantified via changes in CFDA-SE (live) and NucView (apoptotic) FI signals in cultures with P-OSB cells. (a) Change in CFDA-SE FI. (b) Change in NucView FI. (c) Representative brightfield and CFDA-SE (green) image composites. (d) Representative brightfield, CFDA-SE (green), and NucView (red) image composites with scale bars = 150 μm long. 5-10 separate image sets were collected per experimental condition. 2-way ANOVA and Dunnett's multiple comparisons test. 5-10 separate image sets were collected per experimental condition. Two-way ANOVA and Dunnett's multiple comparisons are summarized in Table 2.

sequential order to quantify the amount of NucView signal being expressed by the MM.1S cells in each condition tested throughout the assay. To quantify changes in CFDA-SE and NucView signals, CFDA-SE data was normalized as follows: $\Delta CFDA\ FI = \frac{FI_{t0}-FI_{tn}}{FI_{t0}} \times 100\%$, where the FI at the start of each image set is the greatest. NucView data was normalized as follows: $\left|\left(\frac{FI_{t240}-FI_{tn}}{FI_{t240}} \times 100\%\right) - \left(\frac{FI_{t240}-FI_{t0}}{FI_{t240}} \times 100\%\right)\right|$, where the FI at the end of each image set is the greatest. As MM.1S viability decreases, CFDA-SE FI is reduced due to the fact that dye escapes from cells with compromised membranes and a concomitant increase in NucView signal (as the cell become apoptotic) was observed. NK cell-mediated cytotoxicity against MM.1S cells resulted in a significant difference compared to baseline changes due to photobleaching and death during the experiments, whereas a lack of change in the ΔFI signals with respect to MM.1S controls indicated the presence of viable cells.

Table 2. Statistical analyses for Figure 2.

Condition vs MM.1S Control	10–120 min	130–240 min	10–120 min	130–240 min
	ΔCFDA Signal		ΔNucView Signal	
NK-92MI Control	n/a	n/a	ns	ns
Co-culture	ns	s****	ns	s****
Triple-culture	ns	ns	ns	s****
S/N Primed MM.1S	ns	s****	ns	s****
S/N Primed NK-92MI	ns	s**	ns	s****

2-way ANOVA and Dunnett's multiple comparisons test. A $p < 0.05$ was considered statistically significant. s - significant difference (****$p < 0.0001$, **$p < 0.01$), ns - not significant, n/a - not applicable (i.e. no CFDA signal). All comparisons were made to the MM.1S controls where cell viability was maintained throughout the experiments. *No significant difference* compared to MM.1S control implies no loss of cell viability. *Significant difference* suggest a departure from control arising from a decrease in cell viability.

2.5. Cytokine profiling

Granzymes A and B, perforin, interleukin 6 (IL-6), and interleukin 10 (IL-10) were detected using a Milliplex MAP Human $CD8^+$ T-Cell Magnetic Bead Panel (Millipore Sigma) and read in a Luminex 200 (Millipore Sigma). Data was analyzed with the Belysa™ Software V 1.0. Cytokine data were normalized to prevent bias due to potential cell number variations between experiments. Since IL-6 was detected only in OSB monocultures and not in NK92MI or MM.1S control conditions, it was normalized to the levels in hFOB and P-OSB control conditions, respectively. Likewise, neither MM.1S nor OSB monocultures produced IL-10, hence IL-10 was normalized to the concentration of this cytokine detected in culture conditions of NK-92MI cells alone. Finally, Granzymes A, B, and perforin were normalized to the concentration of these cytokines in the NK-92MI control supernatant as neither MM.1S nor OSB produced these cytokines in monoculture.

2.6. Statistical considerations

A total of 9 experiments (6 with hFOB and 3 with P-OSB) were conducted for imaging studies during which 5-10 separate image sets were collected per experimental condition. All FI data is represented as a mean with standard deviation of all replicates. Two-way ANOVA analysis was used to compare means of experimental conditions across time points. For this comparison, the FI was analyzed and compared between groups at two separate intervals: (1) 10–120 min) and (2) 130–240 min to study early and late effects. Supernatant analysis for cytokine quantification was performed in duplicate and comparisons across conditions were conducted using one-way ANOVA. $p < 0.05$ was considered statically significant. Data was analyzed in GraphPad Prism (V. 7).

3. Results

3.1. hFOB and P-OSB modulate cytotoxicity of NK-92MI against MM.1S cells

Image analyses showed that in the physical presence of hFOB or hFOB supernatant-primed MM.1S, the ΔFI of CFDA-SE (viable cell signal) and NucView (apoptotic cell signal) of MM.1S cells overlapped with that of MM.1S alone control cultures (Figures 1a and 1b). Table 1 summarizes the statistical analyses of the experiments involving hFOB cells. No statistical differences (ns) were found between 10-120 min, or between 130-240 min for the triple culture and supernatant primed MM.1S conditions. Conversely, co-cultures of MM.1S with NK-92MI cells in the absence of hFBO exhibited a ~30% difference in ΔCFDA-SE and ~55% in ΔNucView FIs compared to MM.1S controls (Fig. 1a and b), which was statistically different (****$p < 0.0001$ for ΔCFDA-SE between 10-240 min and ****$p < 0.0001$ for ΔNucView between 130-240 min). When NK-92MI cells were primed with hFOB supernatant (Figures 1a and 1b), both ΔCFDA-SE and ΔNucView signals overlapped with that of MM.1S control condition up to ~100 min (ns, Table 1), after which they run in parallel to the co-culture condition and were significantly different from that of MM.1S control by the end of the culture period (****$p < 0.0001$ between 130-240 min, Table 1). Representative image composites can be seen in Figures 1c and 1d.

Likewise, the ΔCFDA-SE of MM.1S cells in triple-culture with P-OSB was not significantly different and overlapped with that of the MM.1S control (Figure 2a) signal, showing no statistical differences (ns) between 10-120 min or between 130-240 min (Table 2). The ΔNucView signal (Figure 2b), also overlapped with that of MM.1S controls for the first 120 min of the assays however it was significantly different by the end of the culture (****$p < 0.0001$, Table 2), running parallel to the co-cultures. P-OSB supernatants (priming either MM.1S or NK-92MI cells) had minimal effects on the ΔCFDA-SE and ΔNucView FI signals, similar to those captured in co-culture conditions (Figures 2a and 2b), and were statistically significant from the changes experience by MM.1S cells alone by the end of the culture period (Table 2). Representative image composites can be seen in Figures 2c and 2d.

3.2. Culture conditions containing OSB display a cytokine profile that promotes MM survival and hinders NK cell activity

The culture of NK-92MI with hFOB or P-OSB cells resulted in a significant upregulation of IL-6 and IL-10. Figures 3a and 3b show a ~6–7 and ~2.5-fold increase in IL-6 production, respectively, compared to hFOB and P-OSB controls and co-culture conditions. Similarly, IL-10 production was significantly increased in culture conditions containing NK-92MI cells and hFOB (~6-fold) or P-OSB (~1.5-fold) as seen in Figures 3c and 3d.

Lastly, to determine the NK cell killing mechanism of MM.1S cells, we looked at changes in granzyme A, granzyme B, and perforin production in hFOB containing experiments. Both triple-culture and supernatant-primed MM.1S conditions presented with a significant decrease of ~3 and 1-fold respectively in granzyme A and a ~2.5 and 1-fold in the case of perforin, compared to co-cultures (Figures 3e and 3f). Granzyme B was not detected in our cultures.

4. Discussion

MM relapse and progression are in part modulated by cell adhesion–mediated drug resistance conferred by bone marrow microenvironment stromal cells; an established mechanism used by MM cells to survive chemotherapy [19, 20, 21]. In particular, previous studies have shown that cell-cell interactions of MM and OSB can confer drug resistance to MM cells [3, 4, 20]. Beyond drug resistance, Nair-Gupta et al. [22], also demonstrated that cell–cell contact with stromal cells in the bone marrow was implicated in reducing T cell activation and conferred protection of MM and acute myeloid leukemia cells from bispecific antibody-T cell-mediated lysis *in vitro* and *in vivo*. In this brief communication we report for the first time evidence suggesting a safeguarding

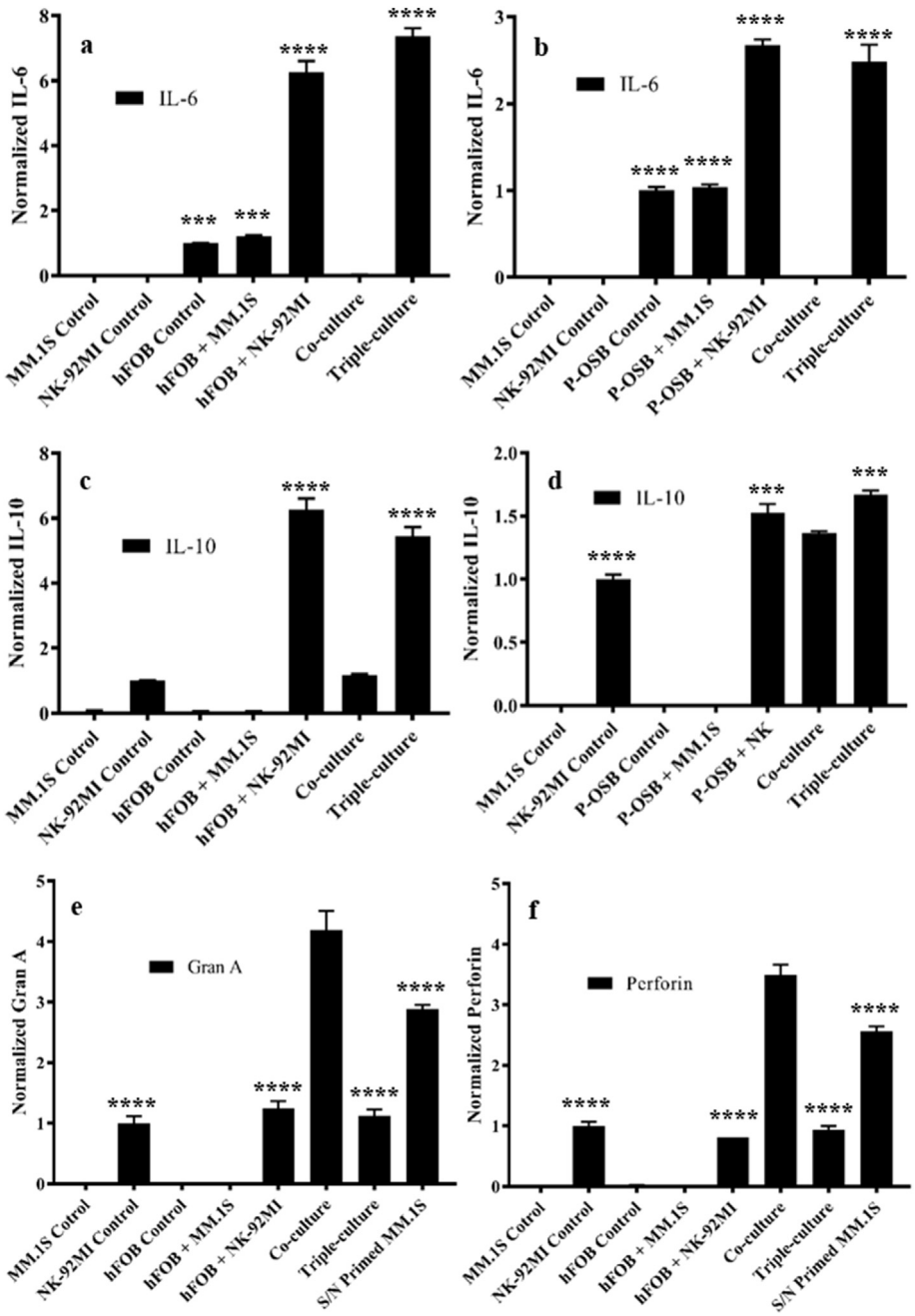

Figure 3. Quantification of cytokine production using multiplex cytokine assay. (a,c) IL-6 and IL-10 fold changes in cultures with hFOB cells. (b,d) IL-6 and IL-10 fold changes in cultures with P-OSB cells. (e,f) Granzyme A and perforin fold changes in cultures with hFOB cells. Statistical analyses were conducted using One Way Anova against co-culture condition followed by Dunnett's multiple comparisons test. $^{****}p < 0.001$ and $^{***}p < 0.01$.

effect of OSB on the cytotoxic activity of NK cells against MM. hFOB in direct culture with MM.1S and NK-92MI cells or priming of MM.1S with hFOB supernatant protected MM.1S cells from NK cell-mediated cytotoxicity. NK-92MI cells primed with hFOB supernatant caused a delay in cytotoxicity as determined by the parallel trajectory of the ΔCFDA-SE and ΔNucView FIs of this condition compared to co-cultures. P-OSB also slowed down NK cell anti-myeloma activity, albeit to a lesser extent than that of hFOB cells, since the ΔNucView FI ran a parallel trajectory to that of co-cultures in the later part of the experiments (i.e., from 130-240min), which was significantly different from MM.1S control cultures. Furthermore, exposure of either MM.1S or NK-92MI cells to P-OSB supernatant did not provide significant protection. The fact that only hFOB supernatant could cause MM.1S to become resistant to NK cell killing suggests, not surprisingly, that hFOB and P-OSB differ in their ability to produce soluble immunomodulatory factors. That notwithstanding, the physical presence of OSB (hFOB or P-OSB) induced NK cell-mediated cytotoxic resistance in MM cells.

The protective mechanism conferred by OSB was studied in part by evaluating the level of IL-6 and IL-10 in our cultures. Bussard et al. [23] demonstrated that murine OSB can be a major source of cytokines in the breast cancer tumor niche and that osteoblast-derived IL-6 was significantly increased when cultures contained breast cancer-derived conditioned media. IL-6 is a pro-inflammatory cytokine reported to confer pro-survival signals to MM cells and reduce NK effector function via

the STAT3 pathway [24, 25, 26]. Known for its pleiotropic effects, IL-10 has also been associated with reduced NK cell activity in cancer [27, 28]. Importantly, IL-10 can act as a proliferation factor for MM cells [26] and increased serum concentrations of IL-10 have been correlated with advanced MM [29].

We, therefore, looked at the relative changes of these cytokines and found that IL-6 and IL-10 were significantly increased in all conditions containing OSB, although to a lesser degree in P-OSB setups, providing a mechanism for the difference in protection levels conferred by hFOB and P-OSB cells. Since IL-10 was not detected in any of the OSB monoculture conditions and NK-92MI cells did not produce IL-6 during the assays, we hypothesize that the observed changes were related to a reciprocal effect through which NK cells modulated the secretion of IL-6 by OSB [23] and OSB regulated the production of IL-10 by NK cells [30]. Interestingly, the upregulations of these cytokines appeared to be associated with an exclusive crosstalk between these two cell types, as triple-cultures presented with comparable fold changes to those obtained in NK + OSB setups. Of note, IL-6 and IL-10 were not detected in MM.1S monoculture controls during the experimental time-frame, further supporting the fact that these cytokines were likely produced by OSB and NK cells, respectively. Our observations also suggest a concomitant action whereby OSB secreted factors could have disrupted the balance between activating and inhibitory ligands on MM cells [6], as hFOB supernatant alone also had a safeguarding effect on MM.1S primed cells.

We also confirmed that the increase in apoptotic MM.1S cells was associated with elevated levels of perforin and granzyme A secretion, which were significantly decreased in experimental conditions containing OSB and, to a lesser extent, primed with OSB media. The overall decrease in cytotoxic granule secretion in the presence of hFOB and P-OSB was therefore congruent with the reduced cytotoxic activity of NK-92MI cells quantified in the time-lapse imaging studies. Interestingly, we have found (*unpublished data*) that anti-apoptotic *BCL-XL* and *BCL2* as well as pro-apoptotic *CHOP* and *CASP3* genes where up- and down-regulated, respectively, in MM.1S cells co-cultured with OSB resulting in an overall pro-survival effect during bortezomib treatment. These results are in agreement with other published studies showing the presence of stromal-mediated activation of pro-survival and anti-apoptotic pathways in MM cells [22, 31].

Lastly, there is evidence to suggest that the extracellular matrix (ECM) of the tumor microenvironment can play an immunomodulatory role on NK cells. ECM molecules such as hyaluronan and MMP-9 have been reported to impair access and cleave tumor ligands that activate NK cells in various tumors [32]. Matrix remodeling has also been hypothesized to contribute to disease progression in MM. In particular collagen, a major component of bone tissue, can exert an inhibitory effect on immune cells that is likely mediated by its binding with the leukocyte-associated Ig-like receptors which are expressed at the surface of most immune cells [33, 34]. A number of studies have focused on developing biomimetic ECM environments that recapitulate the *in vivo* environment of organs and tumors [35, 36]. The utilization of these models could provide further insight on the immunoregulatory role of bone-derived ECM proteins in MM.

5. Conclusions

This research provides new insights towards understanding the immunosuppressive landscape conferred by the osteoblastic niche in the tumor microenvironment of MM, as well as potential therapeutic areas of intervention for circumventing OSB-driven factors that undermine the efficacy and functionality of NK cell therapies against MM. In particular, results from this study suggest a dual immunoregulatory mechanism whereby: (1) the physical contact between OSB and NK cells increased the production of immunosuppressive cytokines IL-6 and IL-10 which likely damped NK cell activity, and (2) soluble factors secreted by OSB caused putative upregulation of anti-apoptotic pathways and or dysregulation of MM cells' activating-deactivating receptors and ligands to enable MM immunity against NK cell-mediated cytotoxicity.

Declarations

Author contribution statement

Christopher Uhl: Performed the experiments; Analyzed and interpreted the data.

Themba Nyirenda: Analyzed and interpreted the data.

David S. Siegel: Contributed reagents, materials, analysis tools or data.

Woo Y. Lee: Conceived and designed the experiments; Wrote the paper.

Jenny Zilberberg: Conceived and designed the experiments; Analyzed and interpreted the data; Contributed reagents, materials, analysis tools or data; Wrote the paper.

Funding statement

This work was supported by the National Institutes of Health, grant#: 1R33CA212806-01A1.

Data availability statement

Data included in article/supplementary material/referenced in article.

Declaration of interests statement

The authors declare no conflict of interest.

Additional information

No additional information is available for this paper.

Acknowledgements

We would like to thank Yan Nikhamin and Dr. Shane Curran from Millipore Sigma for their help with the Milliplex assays execution and analysis.

References

[1] S.V. Rajkumar, Multiple myeloma: 2020 update on diagnosis, risk-stratification and management, Am. J. Hematol. 95 (2020) 548–567.
[2] D. Toscani, M. Bolzoni, F. Accardi, F. Aversa, N. Giuliani, The osteoblastic niche in the context of multiple myeloma, Ann. N. Y. Acad. Sci. 1335 (2015) 45–62.
[3] M.A. Lawson, M.M. McDonald, N. Kovacic, W. Hua Khoo, R.L. Terry, J. Down, W. Kaplan, J. Paton-Hough, C. Fellows, J.A. Pettitt, T. Neil Dear, E. Van Valckenborgh, P.A. Baldock, M.J. Rogers, C.L. Eaton, K. Vanderkerken, A.R. Pettit, J.M. Quinn, A.C. Zannettino, T.G. Phan, P.I. Croucher, Osteoclasts control reactivation of dormant myeloma cells by remodelling the endosteal niche, Nat. Commun. 6 (2015) 8983.
[4] Z. Chen, S. He, J. Zilberberg, W. Lee, Pumpless platform for high-throughput dynamic multicellular culture and chemosensitivity evaluation, Lab Chip 19 (2019) 254–261.
[5] N. Shimasaki, A. Jain, D. Campana, NK cells for cancer immunotherapy, Nat. Rev. Drug Discov. 19 (2020) 200–218.
[6] J. Zhang, H. Zheng, Y. Diao, Natural killer cells and current applications of chimeric antigen receptor-modified NK-92 cells in tumor immunotherapy, Int. J. Mol. Sci. 20 (2019).
[7] Y. Krasnova, E.M. Putz, M.J. Smyth, F. Souza-Fonseca-Guimaraes, Bench to bedside: NK cells and control of metastasis, Clin. Immunol. 177 (2017) 50–59.
[8] A.P. Gonzalez-Rodriguez, M. Villa-Alvarez, C. Sordo-Bahamonde, S. Lorenzo-Herrero, S. Gonzalez, NK cells in the treatment of hematological malignancies, J. Clin. Med. 8 (2019).
[9] T. Iyoda, S. Yamasaki, M. Hidaka, F. Kawano, Y. Abe, K. Suzuki, N. Kadowaki, K. Shimizu, S.I. Fujii, Amelioration of NK cell function driven by Valpha24(+) invariant NKT cell activation in multiple myeloma, Clin. Immunol. 187 (2018) 76–84.

[10] G. Pittari, L. Vago, M. Festuccia, C. Bonini, D. Mudawi, L. Giaccone, B. Bruno, Restoring natural killer cell immunity against multiple myeloma in the era of new drugs, Front. Immunol. 8 (2017) 1444.
[11] J. Xia, S. Minamino, K. Kuwabara, CAR-expressing NK cells for cancer therapy: a new hope, Biosci Trends 14 (2020) 354–359.
[12] Q. Sun, S. Choudhary, C. Mannion, Y. Kissin, J. Zilberberg, W.Y. Lee, Ex vivo construction of human primary 3D-networked osteocytes, Bone 105 (2017) 245–252.
[13] J.H. Gong, G. Maki, H.G. Klingemann, Characterization of a human cell line (NK-92) with phenotypical and functional characteristics of activated natural killer cells, Leukemia 8 (1994) 652–658.
[14] N. Mitwasi, A. Feldmann, C. Arndt, S. Koristka, N. Berndt, J. Jureczek, L.R. Loureiro, R. Bergmann, D. Mathe, N. Hegedus, T. Kovacs, C. Zhang, P. Oberoi, E. Jager, B. Seliger, C. Rossig, A. Temme, J. Eitler, T. Tonn, M. Schmitz, J.C. Hassel, D. Jager, W.S. Wels, M. Bachmann, UniCAR"-modified off-the-shelf NK-92 cells for targeting of GD2-expressing tumour cells, Sci. Rep. 10 (2020) 2141.
[15] S. Greenstein, N.L. Krett, Y. Kurosawa, C. Ma, D. Chauhan, T. Hideshima, K.C. Anderson, S.T. Rosen, Characterization of the MM.1 human multiple myeloma (MM) cell lines: a model system to elucidate the characteristics, behavior, and signaling of steroid-sensitive and -resistant MM cells, Exp. Hematol. 31 (2003) 271–282.
[16] R.E. Goldman-Leikin, H.R. Salwen, C.V. Herst, D. Variakojis, M.L. Bian, M.M. Le Beau, P. Selvanayagan, R. Marder, R. Anderson, S. Weitzman, et al., Characterization of a novel myeloma cell line, MM.1, J. Lab. Clin. Med. 113 (1989) 335–345.
[17] F.A.I. Ehlers, N.M. Mahaweni, T.I. Olieslagers, G.M.J. Bos, L. Wieten, Activated natural killer cells withstand the relatively low glucose concentrations found in the bone marrow of multiple myeloma patients, Front. Oncol. 11 (2021) 622896.
[18] A. Nakamura, S. Suzuki, J. Kanasugi, M. Ejiri, I. Hanamura, R. Ueda, M. Seto, A. Takami, Synergistic effects of venetoclax and daratumumab on antibody-dependent cell-mediated natural killer cytotoxicity in multiple myeloma, Int. J. Mol. Sci. 22 (2021).
[19] F. Fontana, M.J. Scott, J.S. Allen, X. Yang, G. Cui, D. Pan, N. Yanaba, M.A. Fiala, J. O'Neal, A.H. Schmieder-Atteberry, J. Ritchey, M. Rettig, K. Simons, S. Fletcher, R. Vij, J.F. DiPersio, G.M. Lanza, VLA4-Targeted nanoparticles hijack cell adhesion-mediated drug resistance to target refractory myeloma cells and Prolong survival, Clin. Cancer Res. 27 (2021) 1974–1986.
[20] W.C. Chen, G. Hu, L.A. Hazlehurst, Contribution of the bone marrow stromal cells in mediating drug resistance in hematopoietic tumors, Curr. Opin. Pharmacol. 54 (2020) 36–43.
[21] J.S. Damiano, A.E. Cress, L.A. Hazlehurst, A.A. Shtil, W.S. Dalton, Cell adhesion mediated drug resistance (CAM-DR): role of integrins and resistance to apoptosis in human myeloma cell lines, Blood 93 (1999) 1658–1667.
[22] P. Nair-Gupta, S.I. Rudnick, L. Luistro, M. Smith, R. McDaid, Y. Li, K. Pillarisetti, J. Joseph, B. Heidrich, K. Packman, R. Attar, F. Gaudet, Blockade of VLA4 sensitizes leukemic and myeloma tumor cells to CD3 redirection in the bone marrow microenvironment, Blood Cancer J 10 (2020) 65.
[23] K.M. Bussard, D.J. Venzon, A.M. Mastro, Osteoblasts are a major source of inflammatory cytokines in the tumor microenvironment of bone metastatic breast cancer, J. Cell. Biochem. 111 (2010) 1138–1148.
[24] J. Wu, F.X. Gao, C. Wang, M. Qin, F. Han, T. Xu, Z. Hu, Y. Long, X.M. He, X. Deng, D.L. Ren, T.Y. Dai, IL-6 and IL-8 secreted by tumour cells impair the function of NK cells via the STAT3 pathway in oesophageal squamous cell carcinoma, J. Exp. Clin. Cancer Res. 38 (2019) 321.
[25] L. Xu, X. Chen, M. Shen, D.R. Yang, L. Fang, G. Weng, Y. Tsai, P.C. Keng, Y. Chen, S.O. Lee, Inhibition of IL-6-JAK/Stat3 signaling in castration-resistant prostate cancer cells enhances the NK cell-mediated cytotoxicity via alteration of PD-L1/NKG2D ligand levels, Mol. Oncol. 12 (2018) 269–286.
[26] C. Musolino, A. Allegra, V. Innao, A.G. Allegra, G. Pioggia, S. Gangemi, Inflammatory and anti-inflammatory equilibrium, proliferative and antiproliferative balance: the role of cytokines in multiple myeloma, Mediat. Inflamm. 2017 (2017) 1852517.
[27] A. Szkaradkiewicz, T.M. Karpinski, M. Drews, M. Borejsza-Wysocki, P. Majewski, E. Andrzejewska, Natural killer cell cytotoxicity and immunosuppressive cytokines (IL-10, TGF-beta1) in patients with gastric cancer, J. Biomed. Biotechnol. 2010 (2010) 901564.
[28] J.G. Quatromoni, E. Eruslanov, Tumor-associated macrophages: function, phenotype, and link to prognosis in human lung cancer, Am. J. Transl. Res. 4 (2012) 376–389.
[29] C. Pappa, S. Miyakis, G. Tsirakis, A. Sfiridaki, A. Alegakis, M. Kafousi, E.N. Stathopoulos, M.G. Alexandrakis, Serum levels of interleukin-15 and interleukin-10 and their correlation with proliferating cell nuclear antigen in multiple myeloma, Cytokine 37 (2007) 171–175.
[30] S.E. Clark, K.S. Burrack, S.C. Jameson, S.E. Hamilton, L.L. Lenz, NK cell IL-10 production requires IL-15 and IL-10 driven STAT3 activation, Front. Immunol. 10 (2019) 2087.
[31] A. Adomako, V. Calvo, N. Biran, K. Osman, A. Chari, J.C. Paton, A.W. Paton, K. Moore, D.M. Schewe, J.A. Aguirre-Ghiso, Identification of markers that functionally define a quiescent multiple myeloma cell sub-population surviving bortezomib treatment, BMC Cancer 15 (2015) 444.
[32] G.R. Rossi, E.S. Trindade, F. Souza-Fonseca-Guimaraes, Tumor microenvironment-associated extracellular matrix components regulate NK cell function, Front. Immunol. 11 (2020) 73.
[33] F. Asimakopoulos, C. Hope, M.G. Johnson, A. Pagenkopf, K. Gromek, B. Nagel, Extracellular matrix and the myeloid-in-myeloma compartment: balancing tolerogenic and immunogenic inflammation in the myeloma niche, J. Leukoc. Biol. 102 (2017) 265–275.
[34] L. Meyaard, The inhibitory collagen receptor LAIR-1 (CD305), J. Leukoc. Biol. 83 (2008) 799–803.
[35] R. Bascetin, C. Laurent-Issartel, C. Blanc-Fournier, C. Vendrely, S. Kellouche, F. Carreiras, O. Gallet, J. Leroy-Dudal, A biomimetic model of 3D fluid extracellular macromolecular crowding microenvironment fine-tunes ovarian cancer cells dissemination phenotype, Biomaterials 269 (2021) 120610.
[36] J. Kirshner, K.J. Thulien, L.D. Martin, C. Debes Marun, T. Reiman, A.R. Belch, L.M. Pilarski, A unique three-dimensional model for evaluating the impact of therapy on multiple myeloma, Blood 112 (2008) 2935–2945.